Solar-Terrestrial Physics. 2023. Vol. 9. Iss. 3. P. 43–53. DOI: 10.12737/stp-93202306. © 2023
A.S. Potapov, T.N. Polyushkina, A.V. Guglielmi, K.G. Ratovsky, I.S. Moskalev. Published by INFRA-M Academic Publishing House

UDC 550.385.37, 523.31-853
DOI: 10.12737/stp-93202306

Received April 25, 2023
Accepted May 18, 2023

SPECTRAL ANALYSIS OF IAR OSCILLATIONS TO DETERMINE THE VALUE AND VARIABILITY OF THE PEAK ELECTRON DENSITY N_mF2

A.S. Potapov
Institute of Solar-Terrestrial Physics SB RAS, Irkutsk, Russia, potapov@iszf.irk.ru

T.N. Polyushkina
Institute of Solar-Terrestrial Physics SB RAS, Irkutsk, Russia, tnp@iszf.irk.ru

A.V. Guglielmi
Schmidt Institute of Physics of the Earth RAS, Moscow, Russia, guglielmi@mail.ru

K.G. Ratovsky
Institute of Solar-Terrestrial Physics SB RAS, Irkutsk, Russia, ratovsky@iszf.irk.ru

I.S. Moskalev
Institute of Solar-Terrestrial Physics SB RAS, Irkutsk, Russia, hancok@iszf.irk.ru

Abstract. This methodical paper explores the possibility of estimating the peak electron density of the F2-region of the ionosphere (N_mF2) under different conditions, using data on the frequency of spectral bands (harmonics) of the ionospheric Alfvén resonator (IAR) oscillation. We describe a simple technique for tracking the frequency of spectral bands during the day by measuring their position on the plot of the IAR daily dynamic spectrum. Through calculations within the framework of the global ionospheric model IRI-2016, we verify the correctness of the comparison of the frequencies of resonant bands, measured at one point, with data from radio sounding, performed at other points remote from IAR frequency measurement sites at a distance. We propose an algorithm for comparing N_mF2, measured by a radiosonde, with frequencies of spectral lines by precalculating the evaluation factor. It is formed on the basis of a nonlinear combination of the frequencies of the three observed harmonics. Then the time series of this factor is compared with the results of radio sounding, and correlation and regression coefficients, as well as estimation errors are calculated. Using the material on rare cases of round-the-clock observation of IAR oscillations in the winter months of 2011–2012, we trace the dependence of the average error in determining the peak electron density on local time. We present the data on the most favorable local time intervals for determining N_mF2 from IAR harmonic frequencies depending on season. Some additional factors are discussed which affect the accuracy of estimates and determine the frequency range of IAR oscillations.

Keywords: ionospheric Alfvén resonator, spectral bands, oscillation harmonics, electron density maximum, diurnal variations, regression analysis.

INTRODUCTION

In recent decades, the ionospheric Alfvén resonator (IAR) has become widely known as a prominent representative of resonant structures in the atmosphere-ionosphere-magnetosphere system along with such structures as the Schumann [Schumann, 1952], magnetospheric (field-line) [Hasegawa, Chen, 1974; Southwood, 1974], ion-cyclotron [Guglielmi et al al., 2000] resonators, the ionospheric magnetosonic waveguide [Greifinger, Greifinger, 1968], and the waveguide under the plasmapause [Guglielmi, 1979]. Dozens, if not hundreds, of articles have been devoted to the theory and experimentally observed properties of IAR, starting with the works of the discoverers of this phenomenon [Polyakov, 1976; Polyakov, Rapoport, 1981; Belyaev et al., 1987, 1997; Belyaev et al., 1989, 1990, 1999] and their followers [Demekhov et al., 2000; Pokhotelov et al., 2000, 2001, 2003; Bösinger et al., 2002, 2004; Chaston et al., 2002; Lysak, 1991, 2004; Surkov et al., 2004, 2006; Lysak, Yoshikawa, 2006; Semenova et al., 2008; Ermakova et al., 2008, 2011; Simões et al., 2012; Lysak et al., 2013; Dudkin et al., 2014; Baru et al., 2016].

IAR studies provide new information about wave properties of the ionosphere at the junction of the ultralow-frequency (ULF) and extremely low-frequency (ELF) ranges from tenths of Hz to ~10 Hz. The resonant cavity of IAR covers the height interval from the transition region, where the ionosphere passes into the magnetosphere, to the lower ionosphere. The resonator holds standing Alfvén waves in place, whose frequency spectrum is determined by the height distribution of Alfvén velocity and dimensions of the cavity. This opens up the possibility in principle of determining some ionospheric parameters by measuring spectral characteristics of IAR. A detailed description of the morphology of the resonator and properties of its oscillations can be found in the review [Potapov et al., 2021]. IAR plays an important role in the ionosphere-magnetosphere coupling. This resonator may well be open being a part of the general ionospheric-magnetospheric resonator [Guglielmi et al., 2023].

Attempts to verify the possibility and (or) directly use measurements of the spectral structure of IAR oscillations to diagnose the ionosphere as an alternative to its radio sounding have been made since the discovery of the resonator and the theoretical understanding of its physical nature [Belyaev et al., 1990; Yahnin et al.,

2003; Parent et al., 2010; Koloskov, Baru, 2011-2012; Fedorov et al., 2016; Potapov et al., 2016]. The most promising ionospheric parameter in this respect is the F2-region peak electron density N_mF2, where a deep minimum of the vertical Alfvén velocity profile is observed. It is there that most of the wave travel time along the resonator axis accumulates; therefore, the frequencies of IAR harmonics depend most strongly on the main parameter of this region — N_mF2. Nevertheless, it appears in practice that although at certain time intervals the correlation between N_mF2 and the frequency of each of the IAR harmonics is very high, on adjacent intervals it can significantly decrease, thereby leading to large errors in estimating N_mF2.

Potapov and Polyushkina [2020b] made an attempt to solve this problem by applying the multivariate regression analysis involving data on additional parameters. This enabled improving the accuracy of estimating N_mF2, but made it difficult to receive its immediate estimate because some additional parameters cannot be obtained in real-time or even quasi-real time mode. One example is the auroral activity index *AE*.

In this paper, we take a different approach to exploring the possibility of estimating N_mF2 as function of various factors. First, we describe practical ways to track the frequency of oscillation harmonics during the day by measuring the position of resonant harmonic bands in the IAR daily dynamic spectrum. We also assess the validity of comparing the frequencies of resonant bands, measured at one point (observatories Mondy, Uzur, or the station Istok), with radio sounding data from other points (Irkutsk and Norilsk) remote from IAR frequency measurement sites at a certain distance. Then, using the material on rare cases of almost round-the-clock observation of IAR oscillations (which can be made only on certain winter days), we trace the local time dependence of the mean error in estimating N_mF2 and compare it with the mean peak electron density measured by a digisonde. Since, depending on the season, the resonant bands in the daily dynamic spectrum appear at different local times and have different duration, we present data on the intervals most favorable for determining N_mF2 from data on IAR harmonic frequencies during the year. The main purpose of this work is to develop a method of determining the peak electron density in the ionosphere from data on the frequency of IAR harmonics under different conditions and to estimate the errors in such determination, taking into account the ambiguous dependence of the IAR oscillation frequency on N_mF2.

1. DATA AND PREPROCESSING METHODS

The oscillations penetrating from IAR to the Earth surface are classed as geomagnetic pulsations. They are detected by highly sensitive induction magnetometers. The events we discuss in this paper were recorded by a digital induction magnetometer at the mid-latitude station Mondy, located in the territory of Sayan Solar Observatory of ISTP SB RAS. Observations were also made at the mid-latitude station Uzur and the high-latitude station Istok, but they are not used in this paper. The magnetometer LEMI-030 in the station Mondy has the following characteristics. The main element is an induction sensor in the form of a multiturn coil with a core having high magnetic permeability. There is also a pre-amplifier, a set of filters, including a 50 Hz stop filter, an analog-to-digital converter (ADC), and a digital storage. The frequency range of the instrument is 0.001–30 Hz. In the range 1–30 Hz, it has a flat frequency response with a conversion factor of 20 mV/nT. The noise level does not exceed 0.2 pT/Hz$^{1/2}$ at a frequency of 1 Hz and 0.2 pT/Hz$^{1/2}$ at a frequency of 10 Hz. Its ADC has 24 bits; the sampling rate is 64 Hz. For the analysis, we have used output data from two horizontal sensors, oriented from north to south (*X* component) and from east to west (*Y* component). The time was controlled by a GPS receiver.

Digital magnetic recordings in the range 1–8 Hz were processed using a computer code, specially developed for IAR in MATLAB. The program calculates the dynamic signal spectrum from two components and constructs a daily frequency—time spectrogram. The signal intensity at a given frequency at a given time is marked with color. We used a Gabor window 200 s wide with an overlap of 15360 points. From these daily spectrograms we have selected those that display frequency structures characteristic of IAR oscillations, which have the form of spectral bands regularly bending during the day (such a spectrogram is shown in Figure 1). The database with dynamic spectra of IAR for 2009–2020 is available for free on [https://data.kmio.istp.ac.ru].

For this study, we have selected events in which three spectral bands were clearly visible for at least part of the day, from the second to the fourth. Each band corresponds to one of the resonator oscillation harmonics. We did not measure the first harmonic because it is typically noisy due to superposition of the spectral response of Pi1 or Pc1 geomagnetic pulsations, or simply arbitrary noise emissions.

In recent years, a number of papers [Beggan, 2014; Getmanov et al., 2018; Marangio et al., 2020] have been published which propose methods for automatic analysis of the structure of dynamic oscillation spectra, in particular, IAR-type resonance ones. These methods are, however, still far from perfect in terms of natural signals. For example, Marangio et al. [2020] admit that their technique using neural nets works well with geophysical data provided that "they have clearly defined patterns with minimum noise".

In our work, we visually determine harmonic frequencies. To do this, as shown in Figure 1, vertical lines crossing the three harmonics of interest (from the second to the fourth) are drawn from each hour mark in the selected spectrograms. The harmonic frequencies are measured by determining the cursor position indicating the intersection of a vertical line with the harmonic spectral band center. Then, the obtained frequency values are processed using a certain algorithm to calculate the so-called estimation factor Q_{est}; the resulting values are compared with measurements of N_mF2 obtained by radio sounding of the F2-layer critical frequency f_oF2,

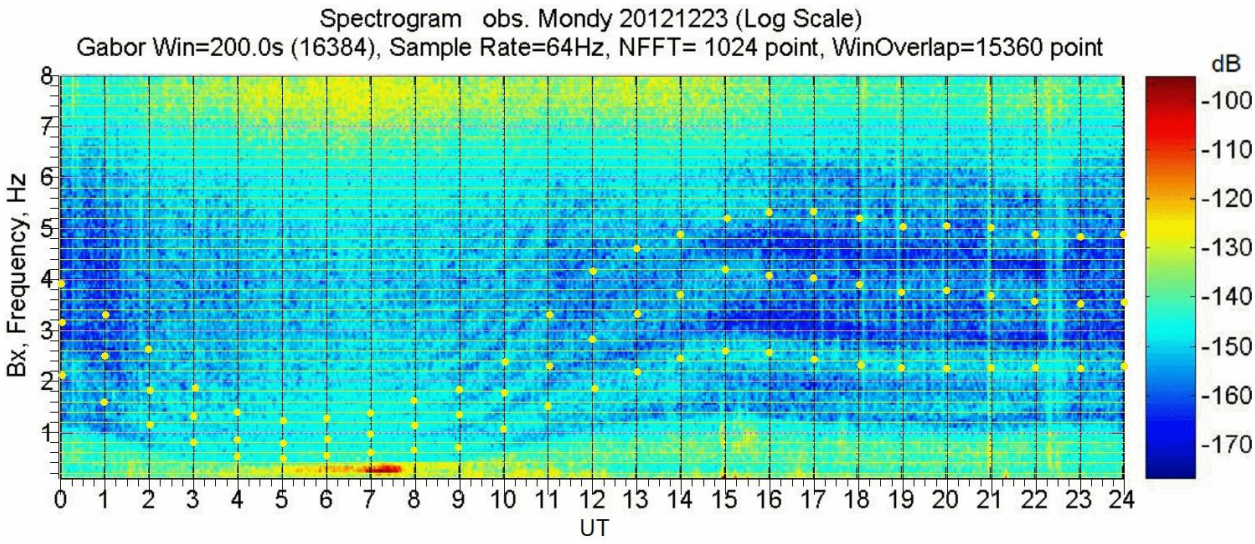

Figure 1. Daily spectrogram of the IAR winter event on December 23, 2012 Yellow dots show harmonic frequencies (from the second to the fourth) for each hour

uniquely related to N_mF2. The F2-layer critical frequency f_oF2 were measured with a digisonde DPS-4 in Irkutsk [Reinisch et al., 1997].

Before the comparison, two important procedures were performed. Firstly, a number of N_m F2 values calculated from f_oF2 were smoothed by the moving average method in order to eliminate the influence of short-period wave disturbances in the radio sounding region. (The resonator properties are assumed to be determined not by local conditions in the ionosphere over the measurement site, but by a much wider region, see below.) Secondly, since we had 15-min measurements of the critical frequency, the series of measurements of IAR harmonic frequencies were converted into 15-min values by interpolating hourly measurements.

By comparing Q_{est} with N_mF2, we calculated Pearson correlation coefficients r, as well as coefficients a, b of the linear regression $N_e=aQ_{est}+b$.

The question arises of whether it is fair to compare N_mF2 obtained by measuring the frequency of the IAR oscillations observed at a point with N_mF2 calculated from radio sounding of f_oF2 at another point located at some distance from the first. In other words, what is the correlation radius of f_oF2 (or N_mF2) along the Earth surface compared to the distance between the measurement points?

There is not much information in the literature about spatial scales (correlation radius) of ionospheric conditions. For instance, Stanislawska et al. [1997] believe that the main ionospheric parameters correlate fairly well at distances of ~1 thousand km. Since in our study the sites of magnetic and radio frequency measurements do not coincide with each other, at the beginning of the analysis we clarified the validity of comparing our measurements. We employed the global ionospheric model IRI-2016, which gives an average typical picture of ionospheric conditions above a selected point on the Earth surface for a given specific year, month, day, and hour of observations. Our magnetic data are obtained at three stations located in the following locations (with geographical coordinates indicated): Mondy (52° N, 101° E), Uzur (53° N, 108° E), and Istok (70° N, 88° E). Radio sounding with digisondes DPS-4 is performed at two observatories: Irkutsk (52° N, 104° E) and Norilsk (69° N, 88° E). Since we are primarily interested in the F2-layer peak electron density, we calculate variations in evening and night (17–05 LT) values of this parameter over all the five stations, located practically in the same time sector, where midnight 00 UT is 06–07 LT, using IRI-2016. It is within the interval 17–05 LT that IAR oscillations are most often observed. Figure 2 exemplifies N_mF2 variations in different seasons of 2018. It is obvious that even during the winter solstice the difference between estimated N_mF2 at the points of interest, according to IRI-216, is small. So, between Irkutsk and Mondy it becomes maximum near 01 LT, but does not exceed 9 %. This is significantly smaller than the typical difference between the densities measured by the ionosonde and the model ones. Thus, DPS-4 data from Irkutsk can be used to compare the peak electron density, estimated from the IAR dispersion bands, with direct radio measurements of the critical frequency (and hence N_mF2) at the observatories Mondy and Uzur. The situation is even more favorable for Norilsk—Istok. The differences there between the IRI-2016 profiles are hardly seen at all (Figure 2). (Note that in Figure 2 and further below we give N_mF2 in mm^{-3}, as opposed to the generally accepted units of N_mF2 measurement — m^{-3} and cm^{-3}).

2. ESTIMATED F2-LAYER PEAK ELECTRON DENSITY FROM MEASUREMENTS OF IAR HARMONIC FREQUENCIES

The initial theoretical formulas for finding the dependence of IAR harmonic frequencies f_n^{IAR} and their frequency scale (the difference between adjacent harmonics)

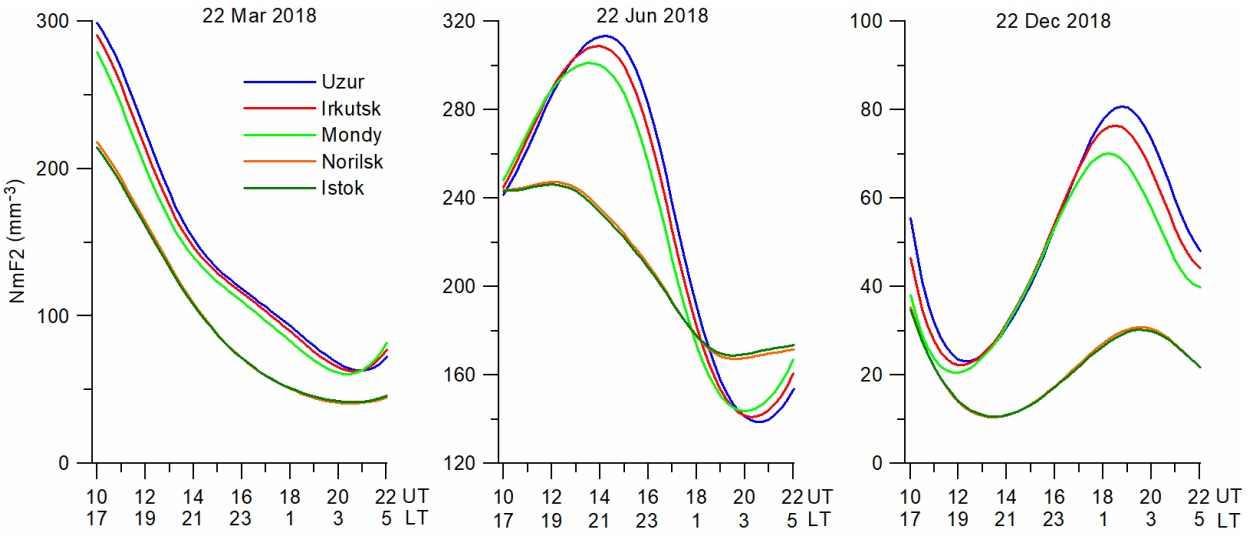

Figure 2. Peak electron density variations in the ionosphere, calculated using IRI-2016 for the equinox and the summer and winter solstices at five stations, where radio sounding was carried out or the IAR harmonic frequencies were measured

Δf^{IAR} on medium parameters have the form [Polyakov, Rapoport, 1981]

$$f_n = \frac{c_{\mathrm{A}}}{2L}(n+\Phi),\ \Delta f = f_{n+1} - f_n = \frac{c_{\mathrm{A}}}{2L}, \qquad (1)$$

or $\Delta f = K/\sqrt{N_{\mathrm{e}}}$, where $c_{\mathrm{A}} = B/\sqrt{4\pi N_{\mathrm{e}} m_{i\,\mathrm{eff}}}$ is the Alfvén velocity; B is the magnetic field at the height of the F2-layer peak electron density (h_{m}F2); L is the characteristic scale of the resonator in the longitudinal direction; $m_{i\mathrm{eff}}$ is the effective mass of ions; n is the harmonic number, $K = B/\left(2L\sqrt{4\pi m_{\mathrm{eff}}}\right)$. In Formula (1), N_{e} is the electron density varying with height, and in fact before $c_{\mathrm{A}} = B/\sqrt{4\pi N_{\mathrm{e}} m_{i\,\mathrm{eff}}}$ in (1) there must be a height integral in order to account for the variations in both N_{e} and B, and m_{eff} with height. But since the frequency of harmonics (as well as the distance between them) is determined by the Alfvén velocity and the longitudinal size of a waveguide, and the Alfvén velocity profile has a deep and sharp minimum in the vicinity of N_{m}F2, while the magnetic field and the effective mass of ions vary with height much slower than N_{e}, for rough estimates we can assume that the frequency generally depends on the Alfvén velocity at peak electron density. These issues are discussed in more detail in [Potapov, Polyushkina, 2020b].

Thus, to estimate N_{m}F2 from Δf^{IAR} measurements, the following formula can be used

$$N_{\mathrm{m}}\mathrm{F2} = \frac{K^2}{\left(\Delta f^{\mathrm{IAR}}\right)^2}, \qquad (2)$$

after determining K^2 from regression analysis of the selected array of simultaneous measurements of N_{m}F2 and Δf^{IAR}.

As for N_{m}F2 estimated from measurements of the frequency of a specific spectral line (harmonic), we have

$$N_{\mathrm{m}}\mathrm{F2} = \frac{K^2(n+\Phi)^2}{(f_n)^2}. \qquad (3)$$

In this case, it is first necessary to estimate the phase parameter Φ. Let us discuss how this can be done. Since the form of the previous formula does not depend on the harmonic number $N_{\mathrm{m}}\mathrm{F2} = K^2(n+\Phi)^2/f_n^2 = K^2(n+m+\Phi)^2/f_{n+m}^2$, where m is an arbitrary integer, it is easy to find that

$$\Phi = \frac{n(1-R)+m}{R-1}, \qquad (4)$$

where $R = f_{n+m}/f_n$. On the other hand, the ratio of the harmonic frequency with the larger number to the harmonic frequency with the smaller number is

$$R = \frac{\Phi+n+m}{\Phi+n}. \qquad (5)$$

So, if n=m=1, Φ=–1/2 at R=3 and Φ=0 at R=2. In the former case, we have a magnetic field antinode of a standing Alfvén wave (type 1) at the lower boundary of the resonator; in the latter, a magnetic field node (type 2), yet IAR oscillations are not observed on the Earth surface. This situation is analyzed in detail in [Potapov et al., 2022a]. It is easy to show that the two variants of harmonic frequency ratios for standing Alfvén waves of types 1 and 2 presented there in the form of triangular matrices were derived from Formulas (4) and (5) given here at Φ=–1/2 and Φ=0 respectively. In the former case, the ratio of harmonic frequencies follows a sequence of odd numbers 1:3:5:9, etc.; in the latter, a set of positive integers 1:2:3:4, etc. In practice, the frequency ratios may deviate from the theoretically predicted ones due to irregularity, nonlinear effects, and other factors. Nonetheless, as shown in [Potapov et al., 2022b], at a mid-latitude observation station they always remain much closer to type 1 standing waves than to type 2 ones.

In fact, there may be two different ways of estimating N_mF2 variations by analyzing spectral bands of IAR oscillations: from the IAR oscillation frequency scale Δf and from the frequency of a separate harmonic, having regard to the phase parameter Φ. The use of any of these methods has its advantages and disadvantages. To estimate N_mF2 from Δf, it is required that several harmonics (4–5 or more spectral bands) be clearly distinguishable in the part of the dynamic spectrum under study.

On the other hand, when estimating an individual harmonic it is not always easy to determine the harmonic number because the selected spectral band may split or merge with another. "Contamination" of the band by irregular low-frequency disturbances is often observed. We have chosen a method for determining from three harmonics — the second, third, and fourth, followed by averaging the results.

3. LOCAL TIME DEPENDENCE OF ERROR IN FINDING N_mF2

To study the local time dependence of the error in finding N_mF2, we have selected 12 winter IAR observation events in January, December 2011 and January 2012. During these events, the spectral bands of the three harmonics of interest were seen in the dynamic spectra for 24 hours. The spectrogram of one of the events is shown in Section 1 in Figure 1. The initial data processing procedure is also described there. It involves measuring hourly frequency values of each of the three harmonics by visually analyzing spectral bands and the linear interpolation of the numerical series of these values to obtain a series of 96 15-min frequency values of each of the harmonics. Further, given that, in view of (3), the peak electron density is expected to be inversely proportional to the square of the harmonic frequency, to ease the subsequent comparison of these frequencies with N_mF2 and the search for correlation and regression coefficients, we calculate the factor $Q_n = (n+\Phi)^2/(f_n)^2$ for each n-th harmonic at each time point. Basing on our previous results obtained in [Potapov et al., 2022a, b], we assume hereinafter $\Phi = -1/2$. Obviously, for the set of harmonics we have chosen, Q_n has the form $Q_2 = 2.25/f_2^2$, $Q_3 = 6.25/f_3^2$, $Q_4 = 12.25/f_4^2$. Further, to obtain the average estimation factor Q_{est}, we simply average the calculated three values of Q_n: $Q_{est} = (Q_2 + Q_3 + Q_4)/3$.

For each of the selected 12 days, we have built data arrays which include the following parameters:

1. A daily series of interpolated 15-min values of Q_{est} averaged over three harmonics.

2. A daily series of 15-min N_mF2 values (mm^{-3}) calculated from DPS-4 f_oF2 measurements in Irkutsk and by moving averaging with a window of 11 points (2.75 hr). In order to maintain a constant number of reference points (96) per day, for the averaging we have used five points (1.25 hr), each from the previous and subsequent days.

3. A daily series of values 1000/h_mF2 measured by the same digisonde and smoothed in the same way.

4. A smoothed series of the total electron content (TEC) in TECU units as measured by the DPS-4 ionosonde. Note that the ionosonde measures the electron density profile only to h_mF2, and TEC is calculated after extrapolating the profile above h_mF2 by the Huang—Reinisch method [Reinisch et al., 2004].

We have used the data on the daily h_mF2 variations and the TEC variations (subsections 3 and 4) only to generally describe ionospheric conditions during each event and do not discuss them further.

Typical daily variations in the listed parameters are indicated by colored lines in Figure 3 for the January 5, 2011 event. Individual harmonic frequency factors Q_n are not shown; only variations in the averaged estimation factor $Q_{est} = (Q_2 + Q_3 + Q_4)/3$ are presented. Figure 3 shows that all four ionospheric parameters — N_mF2, TEC, Q_{est}, and inverse h_mF2 — have similar daily variations, although for different parameters they differ significantly in details. Particularly prominent is the discrepancy in the behavior of the parameters within the local time interval from ~20 hrs to 7 hrs a.m. (13–24 UT). For winter, it is night time. The IAR estimation factor we are first interested in has two main features. (Moreover, they are typical not only for this particular event, but also for other winter cases.) Firstly, before local noon the increase in Q_{est} is 1–2 hours behind the increase in N_e, which underestimates N_mF2 during these hours. Secondly, at night, Q_{est} almost does not respond to changes in N_mF2.

In our opinion, both of these effects are related to the fact that the observed spectral composition depends not on the local conditions above the station, which are reflected in the radio sounding results, but on the longitudinal integral ionospheric characteristics. In the early morning, the region forming the resonator spectrum covers a partially shaded ionosphere with a low electron density; therefore, Q_{est} is underestimated. At night, after the resonator has been formed, its properties and spectral composition are determined by a sufficiently wide region, which includes regions with different N_mF2 values

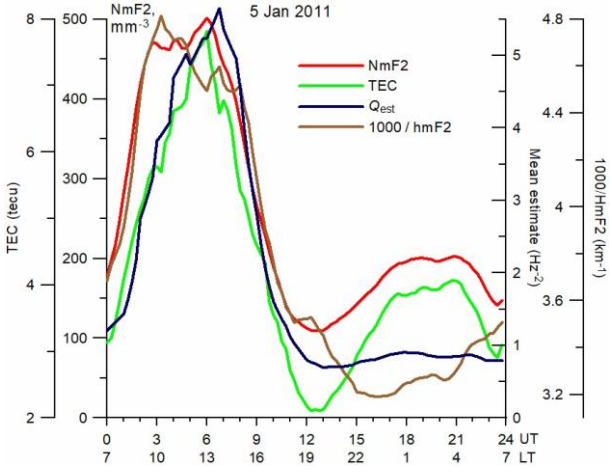

Figure 3. Daily variations in N_mF2 from radio sounding results, TEC, inverse h_mF2 (multiplied by 10^3), and $Q_{est} = (Q_2 + Q_3 + Q_4)/3$, calculated from the frequencies of the second, third, and fourth IAR harmonics

differing from N_mF2 measured above the radio sounding site. These features are typical for winter conditions when IAR oscillations are continuously visible for 24 hours, except for two or three hours around midday, when the IAR spectral bands are difficult to identify. In other seasons, the situation is different; we will back to this later.

To trace the dependence of the IAR spectral characteristics on the time of day, we proceed as follows. We divide the day into three unequal intervals: morning time, including noon (07–13 LT), afternoon interval (13–19 LT), and the period from late evening to early morning (19–07 LT). Then we compare the N_mF2 and Q_{est} variations for each of the selected intervals of the day, as well as during 24 hours for each of the 12 events. For each of the intervals, we calculate the main characteristics of the correlation between N_mF2 and Q_{est}: the Pearson correlation coefficient r_i, where i is the number of the event, i.e. the processed days of IAR observation; the coefficients a_i and b_i of the linear regression $N_m F2^{est} = a_i Q_{est} + b_i$, and the linear dependence coefficient c_i of the regression line $N_m F2^{est} = c_i Q_{est}$ passing through the origin $\left(Q_{est} = 0,\ N_m F2^{est} = 0\right)$. Tables 1–3 list the coefficients obtained for all the winter events considered. The results are shown for the first and second local time intervals, as well as for 24 hours. The correlation between N_mF2 and Q_{est} for the third (night) interval proved to be low and randomly varying from event to event; for a number of events it had a negative sign (anticorrelation), even with a general positive and high correlation according to the data for 24 hours.

The results given in Tables suggest that the correlation between N_mF2 and Q_{est} varies greatly within 24 hours. It is highest in the afternoon (Table 2) when the electron density in the ionosphere decreases. This correlation is less pronounced in the morning (Table 1) when the electron density increases. At night, there is almost no correlation at minimum N_mF2, although, according to round-the-clock observations, the correlation between N_mF2 and Q_{est} remains high. To illustrate these variations, we calculated the errors in estimating N_mF2 from measured Q_{est}, using different versions of the regression equation with coefficients derived by averaging separately over the morning, afternoon, and round-the-clock intervals of all the events.

The results show that the smallest errors in estimating N_mF2 from measured Q_{est} are given by the linear regression equation $N_m F2^{est} = aQ_{est} + b$ with a=62.34 and b=77.56, derived by averaging them for the afternoon interval of all the events. It is significant that the errors are minimal not only for the afternoon, but also throughout 24 hours. The daily average error in determining N_mF2 from the above regression equation is 64.4±13 mm^{-3}. The daily variation of these errors, averaged over all the events, is shown in Figure 4 together with the daily variation of averaged N_mF2.

As discussed above in the description of Figure 3, the increased errors in the morning are associated with a delay in the response of the IAR oscillation frequency to a local increase in the electron density in the ionosphere,

Table 1

Coefficients of correlation r_i, regression a_i and b_i, and linear dependence c_i, their averages and standard deviations (SD) for the interval 07–13 LT

No.	Date	r_i	a_i	b_i	c_i
1	Jan. 23, 2011	0.921	58.7	139	90.8
2	Jan. 05, 2011	0.896	61.9	195	110
3	Jan. 08, 2011	0.868	71.9	235	127
4	Jan. 11, 2011	0.822	35.5	234	77.5
5	Jan. 12, 2011	0.917	36.2	174	63.5
6	Jan. 19, 2011	0.811	49.4	247	109
7	Jan. 20, 2011	0.866	48.1	174	90.1
8	Jan. 22, 2011	0.870	71.1	191	135
9	Dec. 19, 2011	0.864	61.2	314	105
10	Dec. 24, 2011	0.813	53.2	360	104
11	Jan. 07, 2012	0.773	57.6	514	114
12	Dec. 23, 2012	0.982	93.2	50.1	104
Average		0.867	58.2	235	103
SD		0.058	16.0	118	19.9

Table 2

Coefficients of correlation r_i, regression a_i and b_i, and linear dependence c_i, their averages and standard deviations (SD) for 13–19 LT

No.	Date	r_i	a_i	b_i	c_i
1	Jan. 23, 2011	0.991	68.4	60.5	83.8
2	Jan. 05, 2011	0.990	74.6	55.9	88.2
3	Jan. 08, 2011	0.990	67.0	62.9	78.8
4	Jan. 11, 2011	0.989	44.7	97.1	62.8
5	Jan. 12, 2011	0.991	53.9	47.3	62.1
6	Jan. 19, 2011	0.992	60.1	90.6	82.3
7	Jan. 20, 2011	0.958	60.8	65.0	76.0
8	Jan. 22, 2011	0.990	75.7	46.7	89.3
9	Dec. 19, 2011	0.987	58.6	99	69.4
10	Dec. 24, 2011	0.989	54.3	105	65.9
11	Jan. 07, 2012	0.991	62.0	122	73.7
12	Dec. 23, 2012	0.988	68.6	78.8	83.8
Average		0.987	62.3	77.6	76.3
SD		0.009	9.07	24.8	9.59

Table 3

Coefficients of correlation r_i, regression a_i and b_i, and linear dependence c_i, their averages and standard deviations (SD) for 24 hours

No.	Date	r_i	a_i	b_i	c_i
1	Jan. 23, 2011	0.963	71.6	67.8	90.1
2	Jan. 05, 2011	0.932	73.2	107	105
3	Jan. 08, 2011	0.871	74.2	111	100
4	Jan. 11, 2011	0.887	53.8	89.4	73.1
5	Jan. 12, 2011	0.927	45.9	100	65.4
6	Jan. 19, 2011	0.890	78.1	73.3	98.1
7	Jan. 20, 2011	0.923	66.5	69.7	84.9
8	Jan. 22, 2011	0.886	84.2	75.7	110
9	Dec. 19, 2011	0.883	71.4	78.8	82.9
10	Dec. 24, 2011	0.860	66.1	103	80.7
11	Jan. 07, 2012	0.837	72.1	169	92.0
12	Dec. 23, 2012	0.926	60.3	95.5	77.7
Average		0.899	68.1	95.2	88.4
SD		0.036	10.6	28.0	13.5

and this delay is due to a sufficiently large longitudinal extent of the resonator. The rest of the time, from 13 LT to the end of the day, the errors in absolute value are small. The fact that Q_{est} has almost no correlation with electron density at night is explained by two additional factors (besides the longitude of the resonator). First, the spectral bandwidth at this time is large, and variations in their frequency do not exceed the bandwidths, which leads to large errors in measuring the frequency of harmonics. Second, the actual N_mF2 variations measured by the digisonde are low, most often noise-like, and do not exceed the accuracy of radio sounding measurements.

The described results were obtained for winter conditions when the Sun does not rise high at the latitude of the observation station and the illumination of the lower ionosphere is weak even in the afternoon, which allows IAR oscillations to penetrate to the Earth surface. The dependence of the duration of observation of the IAR spectral bands on conditions of illumination of the ionosphere in different seasons is illustrated in detail in Figures 3, 4 in [Potapov et al., 2014]. Already within 40–50 days after the winter solstice, the IAR spectral bands during morning-noon hours become indistinguishable. At the same time, the beginning of the upward fan of bands is shifted to later hours. By the spring equinox, the beginning of the distinguishable spectral structure is within 18–19 LT, and after 2–3 hrs the bands smoothly transform into night ones. In May–July, only small fragments of bands lasting up to three-four hours are visible at night, usually from 23 to 03 LT. Then, everything repeats in reverse order until the next winter solstice.

We have explored the possibility of estimating the peak electron density of the ionosphere from the data on IAR harmonic frequencies for other seasons, at least in those small windows in the daily dynamic spectra when harmonic bands are visible and can be digitized. As an example we show the August 13, 2011 event (Figure 5).

Spectral bands were observed from 14 to 21 UT (21–04 LT). In this short period, we have a very high (r=0.995) correlation between N_mF2 and Q_{est}, but the regression

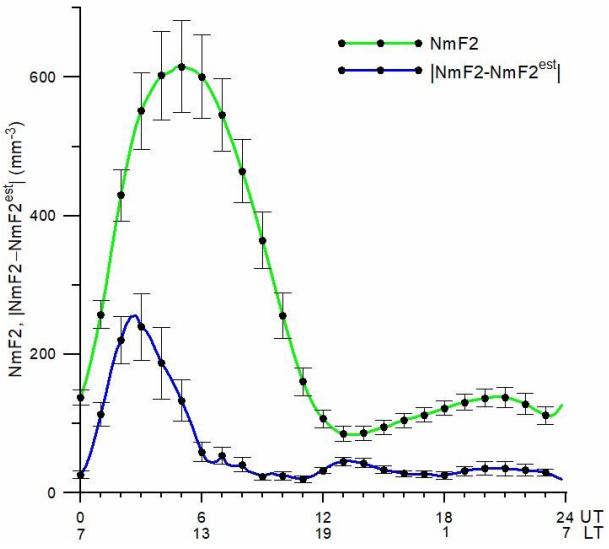

Figure 4. Daily variations in errors, averaged over all 12 winter events, in determining the peak electron density from IAR oscillation spectrum

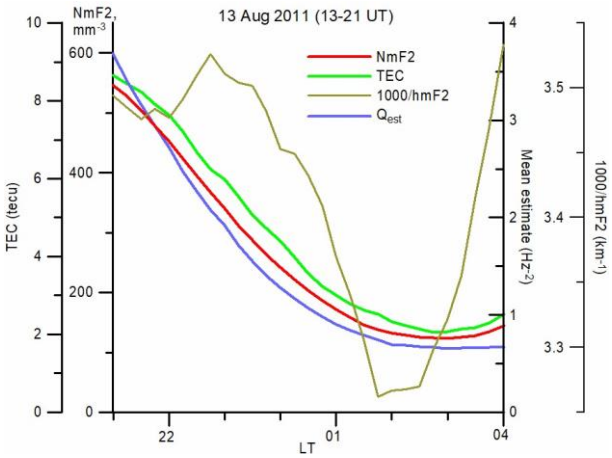

Figure 5. Variations in N_mF2, *TEC*, inverse h_mF2 (multiplied by 10^3), and $Q_{est} = (Q_2 + Q_3 + Q_4)/3$, calculated from the frequencies of the second, third, and fourth IAR harmonics, at the local time night on August 13–14, 2011

coefficients differ significantly from their winter averages. That said, when using them, the mean error in determining N_mF2 from Q_{est} is ~89 mm^{-3}, which is comparable to a similar error for the winter period.

In addition, we performed an independent test of the method, using observational data for the period near the autumnal equinox in September 2011. The procedure was as follows. We selected ten days of the month with clearly distinguishable IAR spectral bands, and during each of the selected days we made two measurements at two time points, measuring the frequency of one of the harmonics at each of the points. The findings are presented in Table 4. As for the winter period, the harmonic frequencies were first recalculated into Q_{est}, which then were used to estimate $N_m F2^{est}$ by the regression equation $N_m F2^{est} = 62.34\, Q_{est} + 77.56$ derived from winter events. The difference was that this time we calculated Q_{est} from measurements of the frequency of one harmonic, and not three as before. As you can see, this did not greatly affect the estimation errors.

Notice that even in June during about half of the nights it is possible to distinguish 3–4 spectral bands within three to four hours. This makes it possible to trace the seasonal and solar-cyclic variations of IAR oscillation frequencies at least for the nighttime (see [Potapov, Polyushkina, 2020a]).

4. DISCUSSION

Initial theoretical formulas (1) are derived within the framework of ideal magnetic hydrodynamics, which allows representing the Alfvén resonator as a one-dimensional stationary oscillatory system. The inhomogeneity and, generally speaking, nonstationarity of the real resonator can, in principle, affect the accuracy of monitoring ionospheric conditions by the method we have proposed. Let us qualitatively discuss this issue.

To begin with, IAR is an open resonator. This means that, unlike closed (volumetric) resonators, the wave field in IAR is bounded in the vertical direction by two ends, i.e. by reflecting elements of the resonator, but in the horizontal direction it is bounded only by a caustic surface.

Table 4

Results of the analysis of estimated N_mF2 on the days close to the autumnal equinox from measured frequencies of individual IAR spectral bands and estimation errors compared to N_mF2 measured by radio sounding

No.	Date (UT)	Time UT/LT	B_x/B_y	Harmonic number	Frequency, Hz	N_mF2, mm^{-3}	Q_{est}, Hz^{-2}	N_mF2^{est}, mm^{-3}	Error, mm^{-3}
1	20110915	17/00	B_x	2	1.1	231	1.86	193	37.9
2		15/22	B_x	3	1.6	356	2.44	230	126
3	20110916	17/00	B_x	4	2.6	257	1.81	191	67.3
4		19/02	B_x	3	2.3	231	1.18	151	80.2
5	20110918	13/20	B_y	4	1.65	470	4.50	358	112
6		12/19	B_y	4	1.4	483	6.25	467	15.6
7	20110920	14/21	B_y	3	1.05	521	5.67	430	89.7
8		15/22	B_y	4	1.7	411	4.24	341	69.6
9	20110921	13/20	B_y	4	1.25	573	7.84	566	7.07
10		14/21	B_y	3	1.05	560	5.67	430	129
11	20110924	12/19	B_y	3	1.05	560	5.67	431	129
12		14/21	B_y	3	1.45	446	2.97	263	183
13	20110926	14/21	B_y	3	1.05	573	5.67	431	142
14		15/22	B_y	4	1.5	434	5.44	417	17.6
15	20110927	13/20	B_x	3	1.25	314	4.00	327	11.9
16		15/22	B_x	4	2.1	240	2.78	251	10.7
17	20110929	17/00	B_x	2	1.3	206	1.33	160	45.8
18		19/02	B_x	4	2.9	160	1.46	168	7.66
19	20110930	11/18	B_y	2	0.5	701	9.00	639	62.6
20		14/21	B_y	4	1.8	367	3.78	313	53.7
							Average		70.0

For simplicity, let lines of the external magnetic field be vertical and the resonator be homogeneous in the horizontal direction. Then, within the framework of ideal magnetic hydrodynamics, modes of the two-dimensional resonator can be represented, for example, as a Gaussian beam of the form $\Phi_n(z)\exp(-ax^2)$. The X and Z axes here are oriented in horizontal and vertical directions, with $z \subseteq [0, L]$. The $\Phi_n(z)$ values are eigenfunctions of the corresponding longitudinal operator. (If c_A does not depend on z, $\Phi_n \propto \sin(\omega_n z / c_A)$, where $\omega_n = \pi c_A n / 2L$, n=1, 3, 5, ...).

There would seem to be no problems since the discrete spectrum ω_n does not depend on the wave field distribution in the resonator cross-section. However, the situation radically changes as soon as we take into account the actual horizontal inhomogeneity of the ionosphere. The discrete spectrum disappears, the oscillation spectrum becomes continuous, the oscillations turn out to be improper (forced) [Guglielmi, Potapov, 1984]. The situation can be remedied if we go beyond the limits of ideal magnetic hydrodynamics and take into account the dependence of the Alfvén wave frequency on the transverse wave vector component. The corresponding corrections to the dispersion equation for Alfvén waves are known as inertial, gyro-frequency, and kinetic corrections. Estimates show that the correction associated with electron inertia prevails at ionospheric heights in the IAR frequency range. An interesting feature of the inertial correction is that the transverse component of the Alfvén wave group velocity is antiparallel to the transverse wave vector component. As a result, the Alfvén wave beam bends in the direction opposite to the horizontal projection of the plasma density gradient. This leads to the fact that the wave field is concentrated in layers and filaments with a reduced plasma density N. Focusing Alfvén waves in structural features of this kind can, generally speaking, lead to the reconstruction of the spectrum discreteness.

From a physical point of view, it is interesting to discuss the possibility of self-focusing of Alfvén waves. It is known that at high latitudes the so-called anabatic polar wind blows, carrying ionospheric plasma into the geomagnetic tail. If an Alfvén wave beam is excited in the polar wind stream, the ponderomotive force slightly increases the wind speed [Guglielmi, Feigin, 2018] and hence reduces the plasma density, thereby causing a peculiar self-focusing of Alfvén waves.

The general picture of the waves is certainly interesting in itself, but let us return to the question we are interested in from a practical point of view, namely: can the transverse field structure in IAR affect the accuracy of our proposed monitoring of ionospheric conditions? We should definitely say that the corrections to the ω_n frequency, associated with the electron inertia, are insignificant. In fact, a relative change in the frequency can be estimated as

$$\delta = m_e c^2 / (4\pi e^2 N a), \quad (6)$$

where a is the Gaussian beam parameter (see above); e and m_e are the electron charge and mass; c is the speed of light [Guglielmi, 1979]. It is easy to show that the dimensionless parameter δ is negligible compared to 1.

In conclusion of this section, let us briefly discuss the question concerning the frequency range of reso-

nance ionospheric oscillations. It is closely related to the question about the IAR autonomy, framed in [Guglielmi et al., 2023]. Indeed, if the IAR range is obviously bounded from below by the frequency of the fundamental oscillation mode, the question about the upper bound is finer. It requires numerical calculation of the reflection coefficient from the upper end of the resonator. Such a calculation can be done by the standard Runge — Kutta method for each specific profile of the vertical Alfvén velocity distribution. It is quite clear that at sufficiently high frequencies the reflection coefficient will be small and the Q-factor of the resonator will be sharply reduced. The rough estimates show that for the typical Alfvén velocity profile the upper bound does not exceed 5–8 Hz, which is quite consistent with the practice in IAR observation.

CONCLUSIONS

In this paper, we have shown the possibility of estimating the peak electron density in the ionosphere by analyzing measured harmonic frequencies of IAR oscillation and have described the practical measurement and analysis procedure. In addition, we have estimated the errors in determining the peak electron density in the ionosphere and its dependence on local time for the winter season. For other seasons, we have indicated approximate local time intervals when IAR spectral bands are observed which are suitable for measuring their frequencies and are then used to estimate the electron density. In the end, we briefly discussed the possible influence of the field distribution in the direction transverse to the resonator axis on the emission spectrum, as well as the question concerning the upper bound of the frequency range of resonance oscillations in the ionosphere.

The work was financially supported by the Russian Science Foundation (Grant No. 22-27-00280) [https://rscf.ru/pr o ject/22-27-00280/]. In terms of conducting observations using the equipment of Shared Equipment Center “Angara” [http://ckp-rf.ru/ckp/3056/], the work was supported by the Ministry of Science and Higher Education of the Russian Federation.

REFERENCES

Baru N., Koloskov A., Yampolsky Y., Rakhmatulin R. Multipoint observations of ionospheric Alfvén resonance. *Adv. Astron. Space Phys*. 2016, vol. 6, no. 1, pp. 45–49. DOI: 10.17721/2227-1481.6.45-49.

Beggan C.D. Automatic detection of ionospheric Alfvén resonances using signal and image processing techniques. *Ann. Geophys*. 2014, vol. 32, pp. 951–958. DOI: 10.5194/angeo-32-951-2014.

Belyaev P.P., Polyakov S.V., Rapoport V.O., Trakhtengerts V.Yu. Finding resonance structure spectrum of the atmospheric electromagnetic noise background within short-period geomagnetic pulsation range. *Doklady AN SSSR* [Reports of AS USSR]. 1987, vol. 297, pp. 840–843. (In Russian).

Belyaev P.P., Polyakov S.V., Rapoport V.O., Trakhtengerts V.Y. Theory for the formation of resonance structure in the spectrum of atmospheric electromagnetic background noise in the range of short-period geomagnetic pulsations. Radiophysics and Quantum Electronics. 1989, vol. 32, no. 7, pp. 594–601.

Belyaev P.P., Polyakov S.V., Rapoport V.O., Trakhtengerts V.Yu. The ionospheric Alfvén resonator. *J Atmos. Terr. Phys*. 1990, vol. 52, no. 9, pp. 781–788.

Belyaev P.P., Polyakov S.V., Ermakova E.N., Isaev S.V. Experimental studies of the ionospheric Alfvén resonator using observations of the electromagnetic noise background over the solar cycle of 1985 to 1995. *Radiophysics and Quantum Electronics*. 1997, vol. 40, no. 10, pp. 1305–1319.

Belyaev P.P., Bösinger T., Isaev S.V., Kangas J. First evidence at high latitudes for the ionospheric Alfvén resonator. *J. Geophys. Res*. 1999, vol. 104, pp. 4305–4317. DOI: 10.1029/1998JA900062.

Bösinger T., Haldoupis C., Belyaev P.P., Yakunin M.N., Semenova N.V., Demekhov A.D., Angelopoulos V. Special properties of the ionospheric Alfvén resonator observed at a low-latitude station (L=1.3). *J. Geophys. Res*. 2002, vol. 107, A10, pp. 1281–1289. DOI: 10.1029/2001JA005076.

Bösinger T., Demekhov A.G., Trakhtengerts V.Y. Fine structure in ionospheric Alfvèn resonator spectra observed at low latitude (L=1.3). *Geophys. Res. Lett*. 2004, vol. 31, L18802. DOI: 10.1029/2004GL020777.

Chaston C.C., Bonnell J.W., Carlson C.W., Berthomier M., Peticolas L.M., Roth I., et al. Electron acceleration in the ionospheric Alfvén resonator. *J. Geophys. Res*. 2002, vol. 107, no. A11, p. 1413.

Demekhov A.G., Belyaev P.P., Isaev S.V., Manninen J., Turunen T., Kangas J. Modeling the diurnal evolution of the resonance spectral structure of the atmospheric noise background in the Pc1 frequency range. *J. Atmos. Solar-Terr. Phys*. 2000, vol. 62, pp. 257–265. DOI: 10.1016/S1364-6826(99)00119-4.

Dudkin D., Pilipenko V., Korepanov V., Klimov S., Holzworth R. Electric field signatures of the IAR and Schumann resonance in the upper ionosphere detected by Chibis-M microsatellite. *J. Atmos. Solar-Terr. Phys*. 2014, vol. 117, pp. 81–87. DOI: 10.1016/j.jastp.2014.05.013.

Ermakova E.N., Kotik D.S., Polyakov S.V. Studying specific features of the resonance structure of the background noise spectrum in the frequency range 1–10 Hz with allowance for the slope of the Earth’s magnetic field. *Radiophysics and Quantum Electronics*. 2008, vol. 51, no. 7, pp. 575–584.

Ermakova E.N., Polyakov S.V., Semenova N.V. Study of the fine structure in the spectrum of low-frequency background noise at mid-latitudes. *Physics of Auroral Phenomena*. 2011, vol. 34, no. 2, pp. 147–150.

Fedorov E.N., Mazur N.G., Pilipenko V.A., Ermakova E.N. Modeling diurnal variations of the IAR parameters. *Acta Geod. Geophys*. 2016, vol. 51, no. 4, pp. 597–617. DOI: 10.1007 s40328-015-0158-9.

Getmanov V.G., Dovbnya B.V., Kornilov A.S. Estimating the frequency and amplitude parameters of the serpentine-emission type of geomagnetic pulsations. *Geomagnetism and Aeronomy*. 2018, vol. 58, no. 4, pp. 523–532. https://elibrary.ru/item.asp?id=35724607

Greifinger C., Greifinger P. Theory of hydromagnetic propagation in the ionospheric waveguide. *J. Geophys. Res*. 1968, vol. 73, pp. 7473–7490.

Guglielmi A.V. *MGD volny v okolozemnoi plazme* [MHD Waves in Near-Terrestrial Plasma]. Moscow, Nauka Publ., 1979, 139 p. (In Russian).

Guglielmi A.V., Potapov A.S. Ob osobennosti polya MGD-volny v neodnorodnoi plasme [Concerning one peculiarity of the MHD-wave field in an inhomogeneous plasma]. *Issled. po geomagnetizmu, aeronomii i fizike Solntsa [Research on geomagnetism, aeronomy and solar physics]*. 1984, vol. 70, pp. 149–157. (In Russian).

Guglielmi A.V., Feygin F.Z. Impact of ponderomotive forces on the Earth’s magnetosphere. *Izv., Phys. Solid Earth*.

2018, vol. 54, no. 5, pp. 712–720. DOI: 10.1134/S1069351318050075.

Guglielmi A., Potapov A., Russell C. The ion cyclotron resonator. *JETP Letters*. 2000, vol. 72, iss. 6, pp. 432–435.

Guglielmi A.V., Klain B.I., Potapov A.S. On the spectrum of ultra-low-frequency oscillations of the ionosphere in the Pc1 range. *Geofizicheskie issledovaniya* [Geophysical research]. 2023, vol. 24, no. 1, pp. 74–84. DOI: 10.21455/gr2023.1-5. (In Russian).

Hasegawa A., Chen L. Theory of magnetic pulsations. *Space Sci. Rev*. 1974, vol. 16, pp. 347–359.

Koloskov A.V., Baru N.A. F-layer critical frequency determination from ionospheric Alfven resonance observations. *Ukrainskii antarkticheskii zhurnal* [Ukranian Antarctic J.]. 2011–2012, no. 10-11, pp. 114–120. (In Russian).

Lysak R.L. Feedback instability of the ionospheric resonant cavity. *J. Geophys. Res*. 1991, vol. 96, no. A2, pp. 1553–1568.

Lysak R.L. Magnetosphere–ionosphere coupling by Alfvén waves at midlatitudes. *J. Geophys. Res*. 2004, vol. 109, A07201. DOI: 10.1029/2004JA010454.

Lysak R.L., Yoshikawa A. Resonant cavities and waveguides in the ionosphere and atmosphere. *Magnetospheric ULF Waves: Synthesis and New Directions. Geophys. Monograph Ser*. 2006, vol. 169, pp. 289–306. Washington: American Geophysical Union Publ., DC, USA, 2006.

Lysak R.L., Waters C.L., Sciffer M.D. Modeling of the ionospheric Alfvén resonator in dipolar geometry. *J. Geophys. Res.: Space Phys*. 2013, vol. 118, no. 4, pp. 1514–1528. DOI: 10.1002/jgra.50090.

Marangio P., Christodoulou V., Filgueira R., Rogers H.F., Beggan C.D. Automatic detection of ionospheric Alfvén resonances in magnetic spectrograms using U-net. *Computers and Geosciences*. 2020, vol. 145, article 104598. DOI: 10.1016/j.cageo.2020.104598.

Parent A., Mann I.R., Rae I.J. Effects of substorm dynamics on magnetic signatures of the ionospheric Alfvén resonator. *J. Geophys.: Res. Space Phys*. 2010, vol. 115, art. no. A02312. DOI: 10.1029/2009JA014673.

Pokhotelov O.A., Pokhotelov D., Streltsov A., Khruschev V., Parrot M. Dispersive ionospheric Alfvén resonator. *J. Geophys. Res*. 2000, vol. 105, no. A4, pp. 7737–7746. DOI: 10.1029/ 1999JA900480.

Pokhotelov O.A., Khruschev V., Parrot S., Senchenkov S., Pavlenko V.P. Ionospheric Alfvén resonator revisited: Feedback instability. *J. Geophys. Res*. 2001, vol. 106, no. A11, pp. 25813–258234. DOI: 10.1029/2000JA000450.

Pokhotelov O.A., Feygin F.Z., Khabazin Yu, Khruschev V.V., Bösinger T., Kangas J., Prikner K. Observations of IAR spectral resonance at a large triangle of geophysical observatories. *Proc. XXVI Annual Seminar "Physics of Auroral Phenomena". Apatity: Kola, Science Center, RAS*. 2003, pp. 123–126.

Polyakov S.V. On the properties of ionospheric Alfvén resonator. *Simpozium KAPG po solnechno-zemnoi fizike* [KAPG Simpozium on Solar-Terrestrial Physics], Book of Abstracts. Moscow, Nauka, 1976, part 3, pp. 72–73. (In Russian).

Polyakov S.V., Rapoport V.O. Ionospheric Alfvén resonator. *Geomagnetizm i aeronomiya* [Geomagnetism and Aeronomy]. 1981, vol. 21, no. 5, pp. 816–822. (In Russian).

Potapov A.S., Polyushkina T.N. Response of IAR frequency scale to solar and magnetic activity in solar cycle 24. *AIMS Geosciences*. 2020a, vol. 6, iss. 4, pp. 545–560. DOI: 10.3934/geosci.2020031.

Potapov A.S., Polyushkina T.N. Estimation of the ionosphere critical frequency without radio sounding. *IEEE Trans. Geoscience and Remote Sensing*. 2020b, vol. 58, no. 7, pp. 5058–5065. DOI: 10.1109/TGRS.2020.2972011.

Potapov A., Polyushkina T., Dovbnya B., Tsegmed B., Rakhmatulin R. Emissions of ionospheric Alfvén resonator and ionospheric conditions. *J. Atmos. Solar-Terr. Phys*. 2014, vol. 119, pp. 91–101. DOI: 10.1016/j.jastp.2014.07.001.

Potapov A.S., Polyushkina T.N., Oinats A.V., Pashinin A.Yu, Raita T., Tsegmed B. The first attempt to estimate the ion content over the ionosphere using data from the IAR frequency structure. *Sovremennye Problemy Distantsionnogo Zondirovaniya Zemli Iz Kosmosa* (Current problems in remote sensing of the Earth from space). 2016, vol. 13, no. 2, pp. 192–202. DOI: 10.21046/2070-7401-2016-13-2-192-202. (In Russian).

Potapov A.S., Polyushkina T.N., Tsegmed B. Morphology and diagnostic potential of the ionospheric Alfvén resonator. *Solar-Terr. Phys*. 2021, vol. 7, iss. 3, pp. 36–52. DOI: 10.12737/stp-73202104.

Potapov A.S., Guglielmi A.V., Klain B.I. Discrete spectrum of ULF oscillations of the ionosphere. *IEEE Transactions on Geoscience and Remote Sensing*. 2022a, vol. 60, art. no. 4600505. DOI: 10.1109/TGRS.2021.3092738.

Potapov A.S., Guglielmi A.V., Klain B.I. Ratio between discrete IAR frequencies from observations in the solar cycle 24. *IEEE Transactions on Geoscience and Remote Sensing*. vol. 60, 2022b, art no. 2004605. DOI: 10.1109/TGRS.2022.3170473.

Reinisch B.W., Haines D.M., Bibl K., Galkin I., Huang X., Kitrosser D.F., Sales G.S., Scali J.L. Ionospheric sounding support of over-the-horison radar. *Radio Sci*. 1997, vol. 32, no. 4, pp. 1681–1694. DOI: 10.1029/97RS00841.

Reinisch, B. W., Huang X.-Q., Belehaki A., Shi J.-K., Zhang M.-L. Ilma R., Modeling the IRI topside profile using scale height from ground-based ionosonde measurements. *Adv. Space Res*. 2004, vol. 34, pp. 2026–2031. DOI: 10.1016/j.asr.2004.06.012.

Schumann W.O. On the radiation free self oscillations of a conducting sphere, which is surrounded by an air layer and an ionospheric shell. *Z Naturforsch*. 1952, vol. 72, pp. 149–155.

Semenova N.V., Yahnin A.G., Vasil'ev A.N., Amm O. Specific features of resonance structures in spectra of ULF electromagnetic noise at high latitudes (Barentsburg Observatory). *Geomagnetism and Aeronomy*. 2008, vol. 48, pp. 36–44. DOI: 10.1007/s11478-008-1005-8.

Simões F., Klenzing J., Ivanov S., Pfaff R., Freudenreich H., Bilitza D., et al. Detection of ionospheric Alfvén resonator signatures in the equatorial ionosphere. *J. Geophys. Res.: Space Res*. 2012, vol. 117, A11305. DOI: 10.1029/2012JA017709.

Southwood D.J. Some features of field line resonances in the magnetosphere. *Planet. Space Sci*. 1974, vol. 22, pp. 483–491.

Stanislawska I., Juchnikowski G., Gulyaeva T. L. Correlation distances based on ionospheric and geomagnetic catalogues. Proc. STP-V Workshop. Hitachi, Japan, 1997, pp. 387–390.

Surkov V.V., Pokhotelov O.A., Parrot M., Fedorov E.N., Hayakawa M. Excitation of the ionospheric resonance cavity by neutral winds at middle latitudes. *Ann. Geophys*. 2004, vol. 22, pp. 2877–2889. DOI: 10.5194/angeo-22-2877-2004.

Surkov V.V., Hayakawa M., Schekotov A.Y., Fedorov E.N., Molchanov O.A. Ionospheric Alfvén resonator excitation due to nearby thunderstorms. *J. Geophys. Res*. 2006, vol. 111, iss. A1, A01303. DOI: 10.1029/2005JA011320.

Yahnin A.G., Semenova N.V., Ostapenko A.A., Kangas J., Manninen J., Turunen T. Morphology of the spectral resonance structure of the electromagnetic background noise in the range of 0.1–4 Hz at L=5.2. *Ann. Geophys*. 2003, vol. 21, pp. 779–786. DOI: 10.5194/angeo-21-779-2003.

URL: https://data.kmio.istp.ac.ru (date of access 19 April 2023).

URL: http://ckp-rf.ru/ckp/3056/ (date of access 19 April 2023).

URL: https://rscf.ru/project/22-27-00280/ (date of access 19 April 2023).

Original Russian version: Potapov A.S., Polyushkina T.N., Guglielmi A.V., Ratovsky K.G., Moskalev I.S., published in Solnechno-zemnaya fizika. 2023. Vol. 9. Iss. 3. P. 52–59. DOI: 10.12737/szf-93202306.

How to cite this article

Potapov A.S., Polyushkina T.N., Guglielmi A.V., Ratovsky K.G., Moskalev I.S. Spectral analysis of IAR oscillations to determine the value and variability of the peak electron density N_mF2. *Solar-Terrestrial Physics*. 2023. Vol. 9. Iss. 3. P. 43–53. DOI: 10.12737/stp-93202306.